Received: 31 January 2021 | Revised: 18 March 2021 | Accepted: 18 March 2021

DOI: 10.1111/jace.17806

Journal of the American Ceramic Society

ORIGINAL ARTICLE

Nanoindentation pop-in in oxides at room temperature: Dislocation activation or crack formation?

Xufei Fang[1] | Hanna Bishara[2] | Kuan Ding[1] | Hanna Tsybenko[2] | Lukas Porz[1] | Marion Höfling[1] | Enrico Bruder[1] | Yingwei Li[3] | Gerhard Dehm[2] | Karsten Durst[1]

[1]Department of Materials and Earth Sciences, Technical University of Darmstadt, Darmstadt, Germany

[2]Max-Planck-Institut für Eisenforschung GmbH, Düsseldorf, Germany

[3]School of Civil Engineering and State Key Laboratory of Water Resources and Hydropower Engineering Science, Wuhan University, Wuhan, China

Correspondence
Xufei Fang, Department of Materials and Earth Sciences, Technical University of Darmstadt, 64287 Darmstadt, Germany.
Email: fang@ceramics.tu-darmstadt.de

Funding information
Deutsche Forschungsgemeinschaft, Grant/Award Number: 414179371, FA 1662/1-1 and DU 424/11-1; ERC Advanced Grant, Grant/Award Number: 787446; Technical University of Darmstadt

Abstract

Most oxide ceramics are known to be brittle macroscopically at room temperature with little or no dislocation-based plasticity prior to crack propagation. Here, we demonstrate the size-dependent brittle to ductile transition in $SrTiO_3$ at room temperature using nanoindentation pop-in events visible as a sudden increase in displacement at nominally constant load. We identify that the indentation pop-in event in $SrTiO_3$ at room temperature, below a critical indenter tip radius, is dominated by dislocation-mediated plasticity. When the tip radius increases to a critical size, concurrent dislocation activation and crack formation, with the latter being the dominating process, occur during the pop-in event. Beyond the experimental examination and theoretical justification presented on $SrTiO_3$ as a model system, further validation on α-Al_2O_3, $BaTiO_3$, and TiO_2 are briefly presented and discussed. A new indentation size effect, mainly for brittle ceramics, is suggested by the competition between the dislocation-based plasticity and crack formation at small scale. Our finding complements the deformation mechanism in the nano-/microscale deformation regime involving plasticity and cracking in ceramics at room temperature to pave the road for dislocation-based mechanics and functionalities study in these materials.

KEYWORDS

crack formation, dislocation, nanoindentation pop-in, oxide, size effect

1 | INTRODUCTION

The scale effect (or "size effect") on the brittleness of solid materials (mainly for brittle solids such as ceramic, glasses, etc.) was first appreciated by Lawn et al.,[1-4] who defined the brittleness incorporating the ratio of hardness and fracture toughness. Later, Gerberich et al.[5,6] revealed and discussed the scale-dependent brittleness transition in silicon. However, the exact role played by dislocations, the one-dimensional defects which are one of the main carriers of plastic deformation in crystals, on the scale-dependent "brittle-ductile transition" was insufficiently discussed for brittle oxides. Contrasting the conventional belief that the majority of oxide ceramics are brittle macroscopically at room temperature,[7] there is abundant evidence for dislocation motion at room temperatures in various ceramics.[8-12] Furthermore, the dislocation-based functionality in oxides is witnessing a research upsurge in recent years. Dislocations are introduced into various oxides to harvest the functional properties. For instance, dislocations have been engineered

in Al_2O_3, ZrO_2, and TiO_2 for electrical conductivity,[13-16] in polycrystalline $BaTiO_3$ for ferroelectric hardening,[17] and in other ceramics such as CeO_2 for reducing the thermal conductivity,[18-20] displaying promising potential to improve the figure of merit for thermoelectric materials.

There are mainly three approaches to introduce dislocations into oxide ceramics. First, using sintering techniques such as flash sintering on TiO_2[21] and yttria-stabilized ZrO_2,[22] or field-assisted hot pressing on $SrTiO_3$.[23] The shortcoming in these sintering processes is that the dislocation structures are poorly controlled. Second, well-aligned dislocations can be produced by bonding crystals such as bi-crystal fabrication,[24-27] which requires strict control of fabrication parameters (temperature, pressure, impurity of the crystals, etc.) for bi-crystals of high quality. Third, dislocations can be introduced into samples by mechanical deformation, for example, via bulk compression at room temperature[28-32] or high temperature,[13,15,33] by near surface mechanical treatment using nanoindentation at a small scale,[34-40] micro-scratching/machining,[41] and so on. While the first two approaches mainly involve processing and fabrication, the third approach relies on the dislocation mechanics of the target ceramic materials under mechanical loading.

Mechanical deformation on bulk samples offers the opportunity to well align the dislocations in the sample on their slip planes.[15,28,33] Nevertheless, one of the most critical issues in bulk deformation of oxide ceramics at room temperature is the crack formation due to the much higher population of pre-existing flaws in the bulk volume[32] in comparison to the small volumes probed at a small scale. Studying the dislocation and crack behavior in these oxides is pertinent as it is desirable to introduce dislocations without cracks in order to harvest the dislocation-based functionalities. In addition, understanding the dislocation-governed mechanics will complement the assessment of the mechanical reliability of such functional materials and devices that are designed to incorporate dislocations.

Many oxides are capable of dislocation-mediated plastic deformation at room temperature at small scales. Page et al.[42] were among the first to point out that deformation in ceramics at very low load (nano)indentation could be mainly dominated by dislocation-mediated plastic deformation, as in the case of sapphire. Further examples are available from nanoindentation tests on MgO,[37,43,44] ZrO_2,[39] ZnO,[45] and $SrTiO_3$.[32,34,35,46] In addition to the examples in conventional instrumented nanoindentation studies with post-mortem surface characterization, the advanced *in situ* TEM indentation study has been employed to directly reveal the dislocation activation in oxides without inducing cracks. For instance, Kondo et al.[27,47] have demonstrated that the dislocations can be induced in $SrTiO_3$ prior to crack formation. Hockey et al.[48-50] investigated the plastic deformation of brittle ceramics such as Al_2O_3 and SiC using indentation and TEM characterization, although the deformation was very often accompanied by crack formation.

The above-reviewed literature of indentation studies on ceramics at a small scale has more or less provided proof that sharp tips such as Berkovich tip or spherical indenter with small tip radius promote dislocation generation while crack formation is suppressed to a certain extent due to locally high hydrostatic compressive stresses. However, there is a lack of systematic and quantitative analysis of the critical criterion to discern these two events. In instrumented nanoindentation, one of the specific focuses in recent years was placed on the nanoindentation pop-in behavior in the load–displacement curve. Pop-in in load-controlled nanoindentation refers to the sudden jump of the displacement during a specific threshold load, signifying the elastic-plastic transition. The nanoindentation pop-in behavior has been extensively studied in recent years in metallic materials[51-58] but has been barely investigated in ceramics materials until very recently.[12,34,59,60] In metallic materials (without thin oxide film formed on the surface[61]) the pop-in indicates dislocation activation. Dislocation activation is believed to be caused either by homogeneous dislocation nucleation[62] under the sharp tip from a volume where no pre-existing defects or dislocations are present or by heterogeneous dislocation nucleation/dislocation multiplication if pre-existing defects or dislocations are available.[51] On the contrary, in ceramics, the corresponding dislocation-governed plasticity during indentation pop-in seems elusive in the shadow of crack formation. Both dislocations and cracks are observed after indentation, making it is difficult to state if crack formation or dislocation-mediated plasticity is dominating. To carefully separate them during dynamic deformation is a challenge where it is particularly difficult to induce dislocations without crack formation. A critical tip radius, R_c, below which the pop-in event correlates only to dislocations without crack formation,[63] is of great interest but yet is ambiguously defined.

In this work, we start by asking the question: for a given oxide ceramic which is ideally free of pre-existing dislocations or surface cracks, which one of the following events occurs first when the near-surface volume is stressed in instrumented indentation: the incipient dislocation nucleation or the incipient crack initiation? The follow-up question is: What is the critical condition/tip radius for the transition to happen between dislocation activation (e.g., dislocation nucleation, multiplication, and motion) and crack formation during indentation pop-in?

With these two questions, we aim to elucidate the competition between the incipient dislocation-based plasticity and incipient crack formation during indentation tests. Many advanced ceramic oxides are being used for MEMS and NEMS devices, meanwhile dislocations are being engineered into oxides to tune the functionalities as briefly introduced before.

It is thus of paramount importance to identify the deformation sequence between dislocation-governed plasticity and crack initiation in ceramic oxides. Such studies would unambiguously contribute to the understanding of dislocation-based mechanics and material's failure in a small-scale deformation of brittle ceramics oxides.

Here, we use the nanoindentation method to investigate the incipient deformation behavior in $SrTiO_3$, which is a prototype perovskite and a candidate for harvesting the functionality[23] and is also a well-known "ductile" oxide which can be plastically deformed even up to about 20% plastic strain at room temperature during bulk compression tests.[64] Three other representative and advanced technology-relevant oxides, that is, Al_2O_3, $BaTiO_3$, and TiO_2 are further examined to validate the generality derived from $SrTiO_3$. α-Al_2O_3 (sapphire) is the hardest oxide used for various semiconductor applications.[65] $BaTiO_3$ is one of the most widely studied ferroelectric oxides, and TiO_2 is widely used as functional oxide for gas sensors, photocatalysis, and photoelectrical devices.[16,66] The following analyses and results are presented on $SrTiO_3$ as a model system, while the accompanying measurements of the other three oxides (see Supplementary Materials) provide the generality of the derived concept.

To be specific, the first pop-in event in the nanoindentation load–displacement curve is adopted as the critical point for interpreting the competing deformation process, dislocation-governed plasticity and crack formation (initiation and/or propagation) in ceramic oxides. In Section 2, we first elucidate the theoretical considerations on nanoindentation pop-in, followed by experimental validation on various advanced oxide ceramics in Sections 3 and 4. Phase transformation will not be the focus in this work, but a short discussion on this issue regarding the incipient plasticity and pop-in will be presented in Section 5 by briefly combing through the literature.

2 | THEORETICAL CONSIDERATION

2.1 | Indentation pop-in

The instrumented nanoindentation pop-in event signifies the elastic-plastic transition during the deformation process. In Figure 1 a representative pop-in event (indicated by the black arrow) is shown on single-crystal $SrTiO_3$. In the following, we assume elastic, isotropic behavior for simplicity, and the elastic behavior prior to pop-in can be described by the Hertzian theory[67]:

$$P = \frac{4}{3} E_r \sqrt{R} h^{3/2} \tag{1}$$

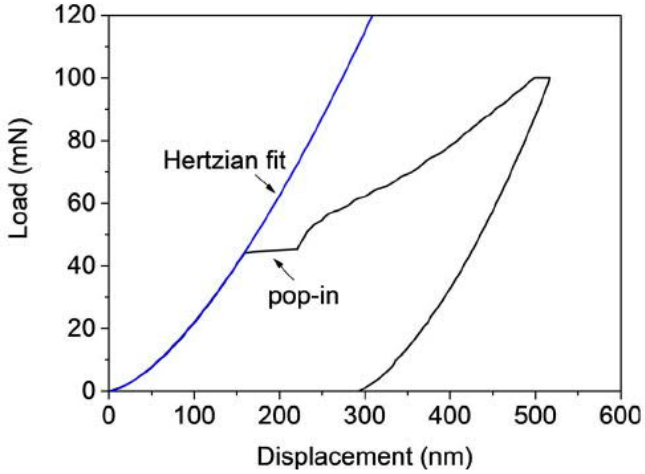

FIGURE 1 Representative nanoindentation load–displacement curve on single-crystal $SrTiO_3$ illustrating a pop-in event, which is the transition from elastic behavior (fitted by Hertzian theory, as indicated by the blue line) to plastic behavior. The nominal tip radius for the spherical indenter is $R = 5$ μm [Color figure can be viewed at wileyonlinelibrary.com]

where P is the load, R is tip radius, E_r is the reduced Young's modulus, and h is the indentation displacement. E_r is calculated from the elastic constants of the indenter and the specimen by[54]:

$$\frac{1}{E_r} = \frac{1-\nu_i^2}{E_i} + \frac{1-\nu_s^2}{E_s} \tag{2}$$

where E is Young's modulus, and ν is Poisson's ratio. The subscripts i and s indicate indenter and sample, respectively.

On the one hand, the maximum shear stress, τ_{max}, induced during the indentation process at the point of pop-in is located about $0.5a$ (a being the contact radius) beneath the surface along the indentation axis, and can be expressed by[67]:

$$\tau_{max} = 0.31 \left(\frac{6E_r^2}{\pi^3 R^2} P_0 \right)^{1/3} \tag{3}$$

where the tip radius R, pop-in load P_0, and reduced modulus E_r are obtained in Equations (1-2).

On the other hand, as mode I fracture dominates in brittle solids, we attend to the maximum tensile stress that is available beneath the indenter at the point of pop-in, which is found to be at the contact ring and is usually considered to result in cone crack ("Hertzian crack") for a blunt spherical tip on brittle solids.[68] This maximum tensile stress is[67,68]:

$$\sigma_{max}^{\text{tensile}} = \frac{(1-2\nu)P_0}{2\pi a^2} \tag{4}$$

where the contact radius at the onset of pop-in is expressed as $a = \left(\frac{3P_0R}{4E_r}\right)^{1/3}$.[67] Hence we have:

$$\sigma_{max}^{\text{tensile}} = \frac{(1-2\nu)(4E_r)^{2/3}P_0^{1/3}}{2\pi(3R)^{2/3}} \tag{5}$$

Combining Equations (3) and (5), it yields:

$$\frac{\sigma_{max}^{\text{tensile}}}{\tau_{max}} = \frac{(1-2\nu)(4E_r)^{2/3}P_0^{1/3}}{2\pi(3R)^{2/3}} / 0.31\left(\frac{6E_r^2}{\pi^3R^2}P_0\right)^{1/3} = \frac{(1-2\nu)}{3\times 0.31} = 0.43 \tag{6}$$

where the Poisson's ratio $\nu = 0.3$ is used. It is interesting to note the tip radius does not appear in Equation (6), which holds true up to the elastic limit, i.e., at the onset of pop-in. Throughout this paper, we adopt the onset of the pop-in as the elastic limit, after which the material will go through incipient inelastic deformation caused by dislocations and/or cracks (depending on the tip radius as will be shown later). In order to clarify the competition between the incipient dislocation-mediated plasticity and the crack-dominated irreversible deformation, the critical stress beneath the indenter tip depending on the tip radius as well as the threshold for shear strength and the fracture strength is explained in the following section.

2.2 | Incipient plasticity and incipient cracking

By incipient plasticity or cracking, we refer to the inelastic deformation events occurring at the onset and during the elasto-plastic transition (e.g., pop-in). Consider a defect-free crystal, the incipient plasticity will be dominated by dislocation nucleation, with probable concurrent occurrence of dislocation multiplication and/or glide motion at room temperature; the incipient cracking will be induced by breaking the atomic bonds and creating new surfaces. Therefore, the competition between the incipient dislocation-mediated plasticity and the crack formation will be determined by the critical stress level reached beneath the indenter tip, with respect to the material intrinsic resistance to plastic deformation (theoretical shear strength being the upper bound) and cracking (theoretical fracture strength being the upper bound). In what follows, we first address these two theoretical upper bounds.

2.2.1 | Theoretical shear strength

Due to the conventional processing of ceramics at high temperatures, it yields very often samples with very low dislocation density. Therefore, in indentation tests with a small indenter tip radius (e.g. R = 90 nm[34]), the maximums shear stress τ_{max} in Equation (3) required to nucleate dislocations in dislocation-free ceramics would approach the theoretical shear strength, which is estimated with an upper bound as $G/2\pi$,[69] with G being the shear modulus. Consider the general case (isotropic) that $G = E/2(1+\nu)$ and $\nu \approx 0.3$, this gives an upper bound of theoretical shear strength as:

$$\tau_{\text{th}} \approx \frac{G}{2\pi} \approx \frac{E}{16} \tag{7}$$

2.2.2 | Theoretical fracture strength without pre-existing cracks

In this case, if a crack occurs during indentation, it will be initiated from the pristine "perfect" surface or near-surface region, and the crack initiation will only be caused by surpassing the material's fracture strength,[70,71] in this case, the cohesive stress, $\sigma_{c-\text{th}}$, that supplies the bonding of the atoms, which can be estimated by[72]:

$$\sigma_{c-\text{th}} = \sqrt{\frac{E\gamma_s}{x_0}} \tag{8}$$

where E is Young's modulus, γ_s the surface energy and x_0 the equilibrium spacing being approximately the distance from two adjacent atomic planes. In what follows we have adopted a much simpler and reasonable estimation of the theoretical fracture strength in the absence of plasticity,that is, $\sigma_{c-\text{th}} = E/10$.[69,73] Later in Section 4, it is demonstrated on $SrTiO_3$ as an example that the estimation of E/10 is even more conservative than Equation (8).

Combining Equations (7) and (8), the ratio between the two theoretical strength is obtained:

$$\frac{\sigma_{c-\text{th}}}{\tau_{\text{th}}} \approx \frac{E/10}{E/16} = 1.6 \tag{9}$$

By comparing Equations (6) and (9), it suggests that when the surface (in an ideal case without pre-existing flaws) is indented with a spherical indenter regardless of the tip radius, the maximum shear stress to reach the theoretical strength will always be first achieved prior to the maximum tensile stress to reach the fracture strength, as illustrated in Figure 2. For linear elastic consideration, the above theoretical prediction holds true for sharp indenter tip probing into sample surfaces with low near-surface imperfection density as in most of the state-of-the-art single-crystal oxides. In such cases, the ideal fracture strength easily exceeds the ideal yield strength, promoting dislocation plasticity prior to crack formation, as will be experimentally validated later in Section 3 using sharp indenter tips on various single-crystal oxides.

Care must be taken, however, when indenters with large tip radii are used, for example, from tens of micrometers for

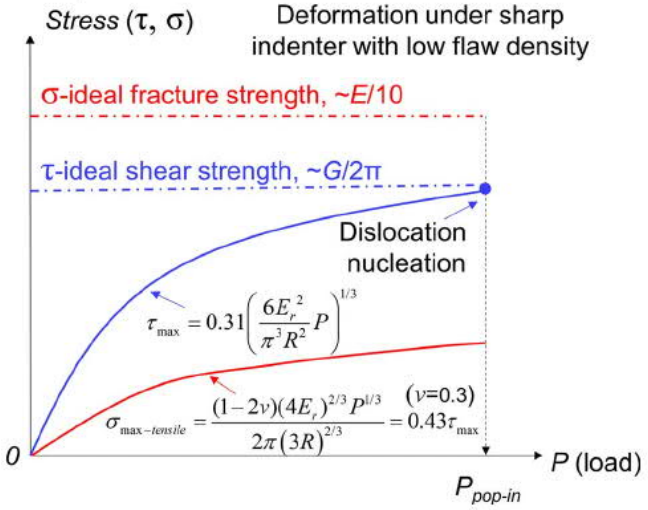

FIGURE 2 Deformation diagram illustrating the maximum shear stress and maximum tensile stress prior to pop-in event under sharp indenter tip in crystals without imperfections. Note that the *x*-axis can also be changed to depth (*h*), with a mathematical conversion according to Equation (1) [Color figure can be viewed at wileyonlinelibrary.com]

large spherical indenters or Vickers indenters (at the apex), the deformation complexity increases for the stress analysis due to the higher probability of probing pre-existing flaws (e.g., pre-existing dislocations or cracks) in a much bigger volume that is stressed. The pre-existing dislocations lower the maximum shear stress for dislocation activation (e.g., heterogeneous dislocation nucleation or motion of the pre-existing dislocations to assist the dislocation plasticity).[32] This may well occur in ceramics fabricated with novel sintering techniques such as flash sintering with a high density of dislocations.[21] On the other hand, the pre-existing cracks would propagate when the applied stress intensity factor reaches the critical value. The presence of pre-existing cracks also lowers the maximum tensile stress required to drive the crack propagation in mode I fracture. These changes involving the flaws will alter Equation (6) since the theoretical values are no longer valid for comparison. The effect of pre-existing defects is discussed later in Section 5.

3 | EXPERIMENTAL PREPARATION

3.1 | Samples

All the oxides used in this study are single crystals. The un-doped $SrTiO_3$ crystals (Shinkosha Co., Ltd.), grown by the Verneuil method with high-purity $SrTiO_3$ powder (99.9 wt% and Sr/Ti = 1.00) and high-purity $SrCO_3$ powder (99.99 wt%), were used for indentation tests on the (001) surface. The sample surfaces were polished by diamond abrasives first and then finished by vibrational polishing with colloidal silica to remove the surface mechanical deformation layer, where an extremely low dislocation density of ~10^{10} m^{-2} is shown by the etch pit study (Figure S1). The surface roughness is checked using atomic force microscopy (AFM, Vecco, Plainview, NY, USA) to ensure a small average surface roughness (e.g., <1 nm for $SrTiO_3$[34]) before the indentation tests. Details on sample preparation of the other three oxides (Al_2O_3, $BaTiO_3$, and TiO_2) for the purpose of validation are provided in the Supplementary Materials.

3.2 | Indentation tests

All indentation tests were performed at room temperature (T = 21°C, with a relative humidity of 33%) on G200 nanoindenter (Keysight Technologies). For continuous stiffness measurement (CSM), a constant strain rate of 0.05 s^{-1} is applied until the predefined maximum displacement is reached. The maximum load and/or maximum displacement for each material and each tip are different but are set slightly higher than the pop-in displacement or load, which have been estimated by carrying out pretests. In some tests especially for large tips (e.g., a spherical tip with a fitted tip radius of R = 25 μm), the tests were immediately stopped manually (pop-in stop tests) after the occurrence of pop-in to avoid the material from being further deformed. Diamond tips (Synton-MDP Nidau, Switzerland) with different tip radii of spherical indenters and sharp Berkovich tips were used. For each test condition, at last 16 indents were performed. Tip calibration was carried out on fused silica before all tests according to the Oliver-Pharr method.[74]

3.3 | Surface structure characterization

The dislocations and cracks in the near-surface region after indentation tests are revealed using high-resolution electron channeling contrast imaging (ECCI), scanning electron microscopy (SEM), and the etch pit method. For $SrTiO_3$, after the indentation tests, the (001) surfaces were chemically etched in 15 mL 50% HNO_3 with 16 drops of 50% HF for ~20 s to reveal the dislocation patterns on the surface. The surface and etch pit patterns were characterized in a scanning electron microscope (SEM, Tescan Mira3-XMH, Brno, Czech Republic) with an acceleration voltage of 5 kV. Details on surface characterization on the other three oxides (Al_2O_3, $BaTiO_3$, and TiO_2) are provided in Supplementary Materials.

4 | RESULTS AND ANALYSES

In what follows, the experimental results obtained on the (001) surface of single-crystal $SrTiO_3$ are presented and

analyzed for representative purposes. The generality of the analysis derived from $SrTiO_3$ is further validated on the other three oxides (Al_2O_3, $BaTiO_3$, and TiO_2), with the detailed results and analyses given in Supplementary Materials.

The post-mortem surface features using etch pits method after indentation tests with different tip radii have been captured using SEM imaging in Figure 3. The fresh dislocations in Figure 3 are induced by deformation as the pre-existing dislocation density is very low (Figure S1). The corresponding load–displacement curves for different tip radii are displayed in Figure 4. For indentation with Berkovich indenter, a higher load than the pop-in load (~0.1 mN at a displacement of ~10 nm) is used to increase the plastic zone size to assist the location of these indents later in SEM. Both Berkovich tip and spherical tip (R = 2 μm) reveal only dislocation activities without any cracks detected, as shown in Figure 3A-B.

Consider the case for the smallest tip radius, R = 100 nm, where no surface imperfections were present. Using

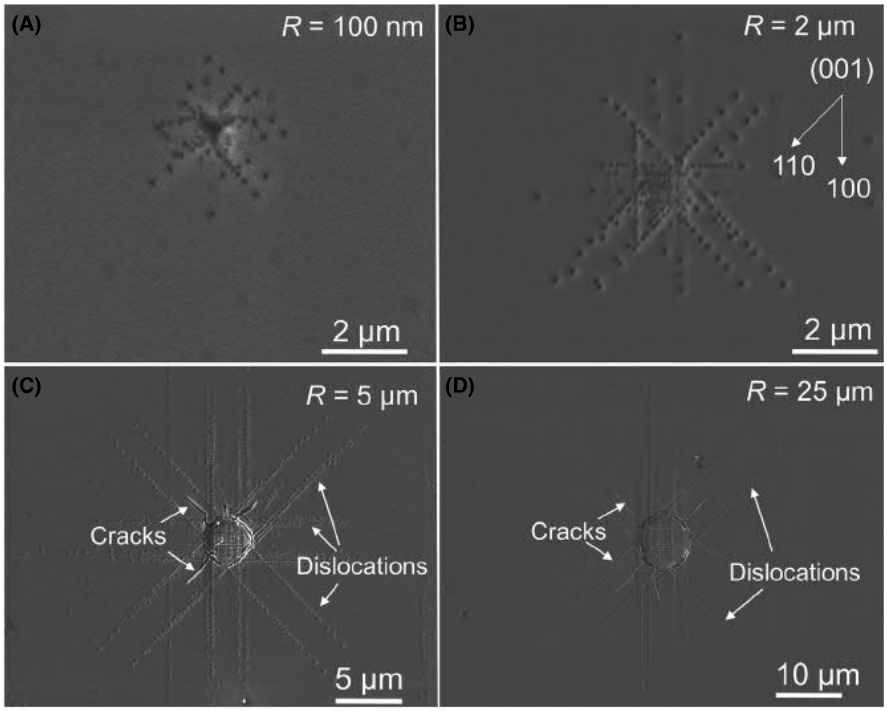

FIGURE 3 SEM images showing the etch pits surrounding the indentation imprints on (001) single-crystal $SrTiO_3$. A transition from dislocation-mediated plasticity in (A,B) to concurrent presence of both crack and dislocations in (C,D) is displayed owing to the different tip radii: (A) Berkovich tip (with an effective tip radius R = 100 nm); (B) Spherical tip (R = 2 μm); (C) Spherical tip (R = 5 μm); (D) Spherical tip (R = 25 μm)

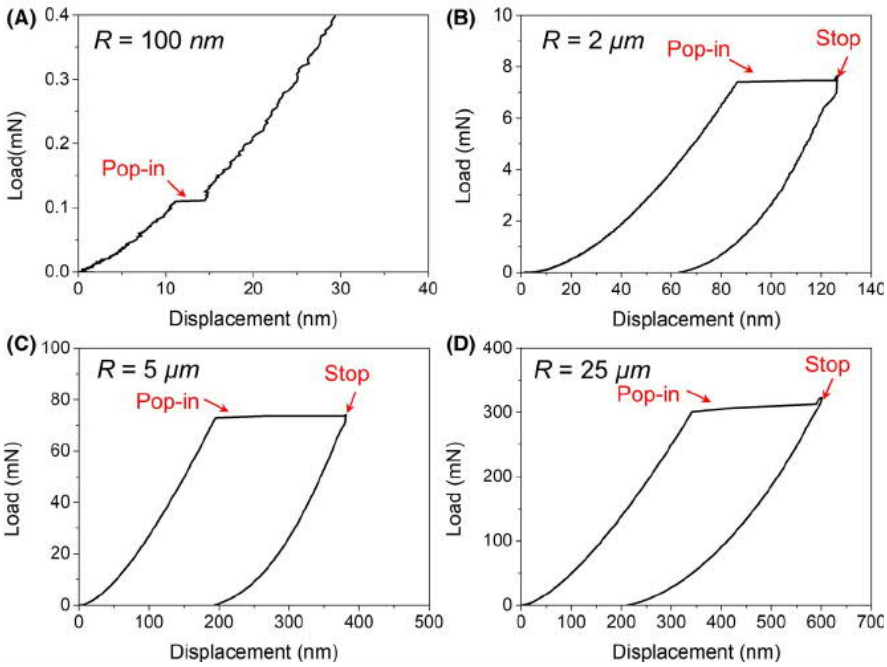

FIGURE 4 Representative load–displacement curves showing pop-in events induced using different tip radii during nanoindentation tests on (001) single-crystal $SrTiO_3$. Pop-in stop tests were performed for larger tip indenters (b-d) to avoid further deformation to induce more potential cracks. Exception is made for Berkovich tip (a) as no cracks are induced when the maximum displacement is set to be 100 nm in this case [Color figure can be viewed at wileyonlinelibrary.com]

Young´s modulus $E = 264$ GPa[28] and the simple estimation of $\sigma_{c-th} \approx E/10$, we have the theoretical fracture strength $\sigma_{c-th} \approx 26.4$ GPa in an ideal case. Moreover, on the one hand, the load-displacement curves give an average pop-in load of $p = \sim 0.1$ mN at a displacement of ~10 nm, corresponding to a contact radius of $a = \sim 40$ nm. With $v = 0.237$[28] and Equation (4), it yields a maximum tensile stress $\sigma_{max-tensile} \approx 5.2$ GPa, which is far below the fracture strength to induce crack formation. On the other hand, for the same boundary condition at pop-in, the maximum shear stress is calculated by Equation (3) to be $\tau_{max} \approx 16.8$GPa, which is identical to the theoretical shear strength $G/2\pi$ (~17 GPa for $SrTiO_3$) in Equation (7).

In this case, it is evident that for the tip with an effective tip radius of $R = 100$ nm, the critical condition of shear strength is reached first, therefore the dislocations will be nucleated prior to crack formation, which is shown in a more straightforward manner by Kondo et al.[27,47] using *in situ* TEM, where a wedge-shaped indenter (with a tip radius of about $R = 100$ nm) was used to induce a large number of dislocations near the surface in $SrTiO_3$ without forming cracks.

The above evaluation, however, does not hold true for a large tip radius, e.g., $R \geq 5$ μm in the case of $SrTiO_3$. For instance, Figure 3C,D shows that both cracks and dislocations are present right after the pop-in events for indenting with tip radii $R = 5$ μm and $R = 25$ μm. Similar results concerning the competition between purely dislocation-dominated process and concurrent dislocation-crack formation depending on the indenter tip radius have been observed in single-crystals Al_2O_3, $BaTiO_3$, and TiO_2 (see Supplementary Materials), demonstrating the generality of the analysis based on $SrTiO_3$.

This size effect on the competing effect of dislocation plasticity and crack formation is considered here as a new indentation size effect (ISE), different from the ISE on depth-dependent hardness,[75] or the size-dependent pop-in phenomena that involve only dislocation activities in metallic materials.[54,56] The ISE on pop-in presented here seems to be exclusively for brittle crystalline ceramics. A detailed discussion on this size effect is presented in Section 5.

5 | DISCUSSION

5.1 | Size effect on the crack formation during indentation pop-in

The pop-in size effect in brittle oxides described in the preceding section can be attributed to several influencing factors. Of most interest is the crack formation during indentation pop-in under larger indenter tips, as evidenced directly after the pop-in stop tests. In brittle solids, there are several prevailing theories concerning the crack formation during indentation. Here we first briefly summarize these theories and then a correlation between these theories and our experimental results will be made.

5.2 | Crack propagation from pre-existing cracks

In brittle solids, the pre-existing cracks or flaws are detrimental as they can serve as stress concentrators. When the applied stress intensity factor reaches the critical value, the cracks propagate. Take mode I fracture in brittle solids as an example, the maximum tensile stress at the contact edge during indentation, when meeting locally pre-existing crack(s), would promote the crack propagation (forming circular or cone cracks) when the stress intensity factor from external loading (K_a) reaches the critical value (K_{Ic}), as illustrated by case 2 in Figure 5. The crack length, in an ideal case, when the crack orients itself perpendicular to the maximum tensile stress, can be estimated by the following equation:

$$\sigma_{max-\text{tensile}} = \frac{K_{Ic}}{Y\sqrt{c}} \tag{10}$$

where K_{Ic} is fracture toughness, c is the crack length, Y is a geometry factor and for simplicity is taken as $Y = \sqrt{\pi}$. Recalling the expression for the maximum tensile stress in terms of the pop-in load, reduced modulus, and tip radius in Equation (5), it yields:

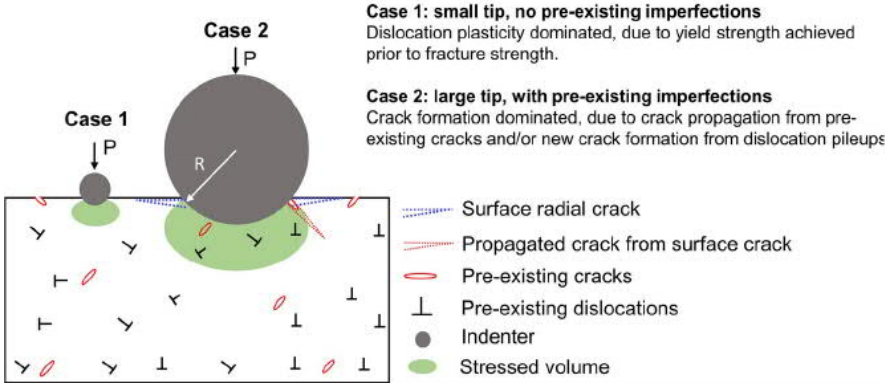

FIGURE 5 Schematic illustration of the indentation size effect related to crack formation in brittle ceramics oxides. The competing effect between the dislocation plasticity and crack formation is closely dependent on the indenter tip radius and the pre-existing defects [Color figure can be viewed at wileyonlinelibrary.com]

$$\sigma_{max-\text{tensile}} = \frac{K_{\text{Ic}}}{\sqrt{\pi c}} = \frac{(1-2\nu)(4E_{\text{r}})^{2/3} P_{\text{pop-in}}^{1/3}}{2\pi\,(3R)^{2/3}} \quad (11)$$

Therefore the critical crack length, c_0, can be estimated by the following equation:

$$c_0 = \left(\frac{K_{Ic}}{\sqrt{\pi}}\right)^2 \left(\frac{2\pi\,(3PR)^{2/3}}{(1-2\nu)(4E_r)^{2/3}P}\right)^2 = \left(\frac{K_{Ic}}{\sqrt{\pi}}\right)^2 \left(\frac{2\pi}{(1-2\nu)P}\right)^2 \left(\frac{3PR}{4E_r}\right)^{4/3} = 4\pi \left(\frac{K_{Ic}}{(1-2\nu)P}\right)^2 a_0^4 \quad (12)$$

where $a_0 = \left(\frac{3PR}{4E_{\text{r}}}\right)^{1/3}$ is the contact radius. Equation (12) is equivalent to the Griffith energy approach[63] if $K_{\text{Ic}}^2 = 2E\gamma_{\text{s}}$ is taken for brittle solids. Note this holds true for linear elastic fracture in the absence of crack tip blunting, as in the case of most ceramics where no crack tip dislocation emission is observed at room temperature.

Take single-crystal $SrTiO_3$ as an example, the sample is indented with tip radius $R = 25$ μm, $P \approx 300$ mN at the pop-in event, $\nu = 0.237$, $E_{\text{r}} = 225$ GPa, $K_{\text{Ic}} = 1$ MPa·m$^{1/2}$,[76] we can estimate the crack length c to be about 45 nm, meaning that a minimum crack length of 45 nm is required for a crack to propagate when the pop-in occurs. Such cracks seem not to exist for single-crystal $SrTiO_3$ of high-quality surface as no such features were detected in the AFM images. The argument based on Equations (11-12) applies for other brittle oxides as long as the corresponding material parameters are provided. Note that if the pre-existing cracks are responsible for the crack formation, due to the maximum tensile stress distribution and a higher chance of probing pre-existing cracks, the cracks are most likely to be evidenced as circular cracks (or cone cracks/Hertzian cracks[68,73]) under large indenter tips, although the formation of median and radial cracks could complicate the isolation of the circular cracks, as shown in Figure 3C,D. In this case, the density and distribution of the pre-existing cracks on the surface will also be critical.[77] However, at this stage, it is remains uncertain whether the presence of pre-existing cracks and their influence for large spherical tip can be completely ruled out, especially for hard materials such as Al_2O_3. For a more comprehensive discussion, we also include the existence of pre-existing cracks in Figure 5.

5.3 | Shear band/fault formation as crack nuclei

Besides the crack propagation from the pre-existing flaws, it was proposed that the formation of shear fault (especially in glasses), which is akin to a shear crack, could serve as crack nuclei and propagate into the subsurface under critical conditions, so as to relax the contact pressure underneath indentation.[3,4,78-81] It was discussed by Lawn et al.[4] that the shear fault surfaces would follow the curved shear stress trajectories in isotropic materials such as glasses or fine-grain polycrystals, while the faults would follow more along the weak crystallographic planes in single crystals. Due to the limited slip systems and a rather high lattice friction stress in most ceramic oxides, the fault patterns in such materials tend to be strongly localized around the indentation imprints. The interactions between different shear fault surfaces result in local high stress concentration sites which are in favor of the initiation of ensuing radial cracks, as experimentally shown in Vickers indentation induced cracks in glasses.[4,80] Similar operating mechanisms have been reported in nanoindentation tests in semiconductor materials such as Si and GaAs[82,83] combined with post-mortem TEM examination, but median cracks were more often induced.

It is worthy of note that in crystalline materials such as oxides and semiconductors, the shear fault surfaces correspond to the slip planes. Therefore, a more detailed examination of the dislocation interactions within these slip planes is of great interest to understand the dislocation-based crack formation and propagation.[63]

5.4 | Crack initiation from dislocation pileup

In addition to the above two mechanisms, compelling experimental observation has suggested crack initiation from dislocation pileup in ceramic materials. In comparison to metals, most ceramic materials have only limited independent slip systems (very often only two[84]) at room temperature. A direct consequence of limited-slip systems in oxides is that the allowed arbitrary plastic strain without change in volume is greatly suppressed.[85] This means that in the highly confined local deformed region in nanoindentation test, cracks may be formed due to dislocation pileups. For instance, based on the cross-sectional observation of the crack formation and dislocation slip patterns, Hagan[79] proposed the Vickers indentation induced median crack formation in LiF was due to the intersecting of the dislocations on the $\{110\}_{45°}$ slip planes, where the angle 45° indicates the inclination of the slip planes with respect to the plane being indented. Farber et al.[86] performed elevated-temperature indentation on {111} planes in 21 mol% Y_2O_3 fully stabilized ZrO_2 and investigated the Lomer-type dislocation pileups using TEM. They observed crack formation from the interaction between the slip bands. Crack arising from slip bands was also observed in MgO single crystals in bulk compression tests by Stokes et al.[87] and Argon et al.[88] Very recently, Fang et al.[63] studied the dislocation pileups induced by spherical indenter tip on (001) plane of single-crystal $SrTiO_3$. By choosing a proper spherical indenter tip radius ($R = 2$ μm), they captured the

crack initiation due to dislocation pileups using the etch pit method. The number of dislocations was quantitatively evaluated for crack initiation based on the theory of Zener–Stroh crack formation.[89] The correlation between the theory and experimental observation suggested that a pileup of about 20 edge dislocations is sufficient to initiate a crack along the {110} plane.

In short, the discussion in this section suggests that in oxides that exhibit dislocation plasticity, the radial cracks are most likely formed due to dislocation pileup, whereas the circular cracks have a more complicated source, which could be either the pre-existing cracks or the dislocation pileups beneath the indenter. Moreover, median cracks have not been observed in "ductile" ceramics such as $SrTiO_3$ by successive polishing and etching[35] after nanoindentation tests.

5.5 | Critical tip radius R_c

It is of great interest for us to theoretically determine or estimate the critical tip radius R_c at which the concurrent crack formation and dislocation-based plasticity occur during the pop-in event. As below this critical tip radius, it is expected that purely dislocation-governed plastic deformation prevails, avoiding the complications of crack formation so that efforts of functionality measurement (e.g., electrical conductivity) can be carried out purely on dislocations. Yet it is no easy task to determine the R_c as the boundary conditions would have to involve and must be dependent on the target material (different deformation mechanisms, slip systems, different lattice friction stress, Burgers vector), sample surface condition (distribution and density of pre-existing defects due to sample preparation[90]), chemical environment (humidity, surface chemistry, reducing atmosphere, etc.), loading rate, tip material (harder diamond tip or softer sapphire tips), and machine dynamics[63,91] in load-controlled machines. In addition, the complexity lies in the concurrent plastic deformation and crack formation during the pop-in event for large indenter tip, making it challenging to discern the sequence of these two deformation processes at the on-set of pop-in. Out of the four oxides we were only able to discern the deformation sequence in $SrTiO_3$.[63] We intend to address these complexities on the critical tip radius in future works with other well-defined materials, controllable surface quality (e.g., various previous dislocation density and crack density), and test conditions.

The discussions above are summarized in Figure 6. It has now become clear that for tips smaller than R_c, the nanoindentation pop-in corresponds to purely dislocation-governed plasticity, as schematically shown in Figure 6A,B. Noticeably, for extremely small tips ($R << R_c$), a critical load P_c (larger than the pop-in load P_0) exists at which cracks start to initiate from the dislocation pileup. For instance, for a sharp Berkovich indenter (with an effective tip radius of $R \approx 100$ nm), the pop-in load is about $P_0 \approx 0.1$ mN, while the load for inducing cracks can be as high as $P_c \approx 3$ mN.[35] For spherical tip (with an effective tip radius of $R = 2$ μm), the pop-in load is about $P_0 \approx 6$~7 mN, while the load for inducing

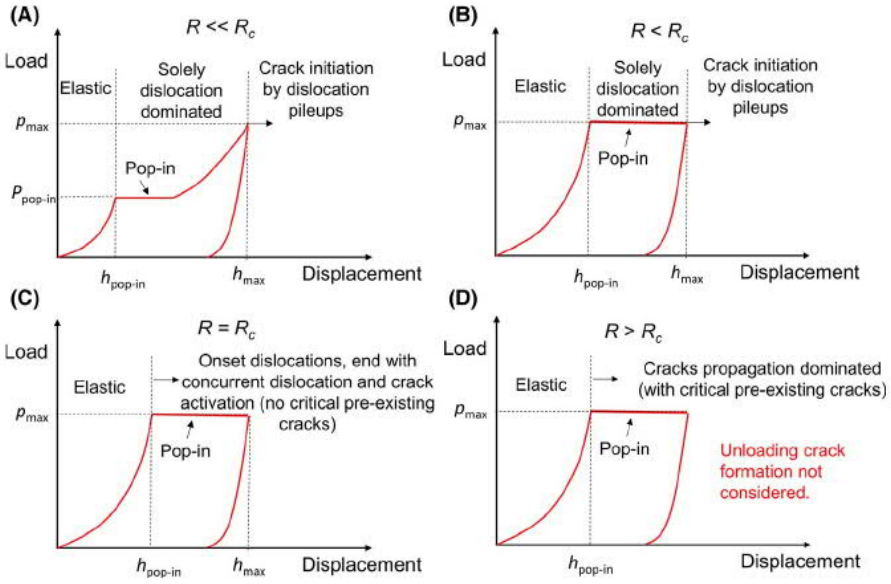

FIGURE 6 Schematic load–displacement curves showing various scenarios concerning dislocation activity and crack formation during indentation pop-in: (A) $R << R_c$, pop-in corresponds to purely dislocation activities, further loading after pop-in involves still only dislocations without crack formation; (B) $R < R_c$, pop-in corresponds to purely dislocation activity, but further loading after pop-in could immediately induce crack formation; (C) $R = R_c$, pop-in corresponds to concurrent dislocation activity and crack formation, with post-mortem observation right after pop-in stop tests showing both dislocation and crack features; (D) $R > R_c$, pop-in corresponds to crack formation while dislocation activity is not dominating [Color figure can be viewed at wileyonlinelibrary.com]

cracks is $P_c \approx 11$ mN.[63] On the other hand, when the tip radius is larger than R_c, concurrent crack formation and dislocation activities are expected during the pop-in event. For larger tips, it is worth noticing that the pop-in distance is also much larger (e.g., Figure 4 and Figure S4, Figure 6). Such a large jump distance, as clearly shown by the post-mortem surface characterization, cannot purely be accommodated by dislocation activities alone due to the limited plasticity. Concurrent crack formation is triggered to accommodate the large pop-in jump. It is also worth pointing out that, no pop-in will be observed if the pre-existing dislocation/defect density in the near-surface region is too high, which is beyond the scope of this study.

5.6 | Generality of the theory: size-dependent brittle-to-ductile transition at room temperature

The generality of the analysis based on $SrTiO_3$ has been validated on Al_2O_3, $BaTiO_3$, and TiO_2. Now we turn to a much broader view of ceramic materials. Previous studies using instrumented nanoindentation on various ceramic oxides such as MgO,[37,43,44] ZrO_2,[39] and ZnO[45] have provided experimental evidence that even brittle oxides deform purely plastically with dislocations under sharp indenter tips (Berkovich tips or small spherical tips). Many other types of ceramics, such as alkali halides, for example, LiF[92] and CaF_2,[40] carbides such as SiC,[42,93] borides such as ZrB_2,[94] sulfides such as ZnS,[12] exhibit also dislocation-governed plasticity during tests with sharp indenters, although a densification process accompanying dislocation activation was sometimes observed. Yet, this dislocation/crack competition-related indentation size effect in pop-in was not explicitly discussed in detail in literature. In the majority of these mentioned studies, cracks were very often found to accompany the deformation process due to the fact that the indentation load was set to a very large value, or indenters with a large radius ($>R_c$) were used, for example, in $LiNbO_3$ and $LiTaO_3$.[95]

Our experimental and theoretical approach based on ceramic oxides is expected to apply for other types of ceramic materials, as have been mentioned previously on, e.g., carbides[93] and borides[94] at room temperature using nanoindentation tests. The essence of the crack-related indentation size effect or the indentation size-dependent brittle to ductile transition is that the shear strength is reached prior to the fracture strength at ever-decreasing small scale with lower flaw density. It is worth mentioning that the size-dependent ductile to brittle transition has been previously reported in Si using nano-/micro pillar compression at room temperature by Östlund et al.,[96] who showed that as the diameter of the pillar decreases below a critical size (310 to 400 nm), the pillar deforms fully ductile without cracking, which is comparable to that of metals. In contrast, cracks were always present when the pillar diameter is larger than 400 nm. A model based on dislocation shielding was proposed to explain this transition.[96]

Based on the above discussion, it is suggested that with a small load and a small indenter tip radius, there is a window to introduce only dislocations with forming cracks in the ceramic oxides. Within this window, it calls for further investigation in both dislocation-based mechanics and functionalities in oxides.

5.7 | Phase transformation and shear amorphization

So far, we have excluded phase transformation as it is irrelevant for the selected four oxides in this work. However, for the sake of completion, we note that phase transformation in brittle ceramic materials could also result in nanoindentation pop-in due to the sufficiently high levels of hydrostatic compression beneath the indenter. Examples of such have been reported in GaAs.[97,98] Another well-known example is Si, in which the incipient plasticity indicated by indentation pop-in has long been attributed to the phase transformation.[99,100] However, Minor et al. used *in situ* nanoindentation in TEM and confirmed that the incipient plasticity is dominated purely by dislocations in <100> n-type single-crystal Si samples that were fabricated lithographically.[101,102] It is also worth noting that phase transformation could also result in the so-called "pop-out" during unloading, as briefly reviewed on Si by Lawn et al.[4] In addition, a most recent work by Reddy et al.[59] verified that the nanoindentation pop-in for B_4C with strong covalent bonds is resulted from the dislocation-mediated shear amorphization.

6 | CONCLUSION

Through the nanoindentation pop-in study with different tip radii on model material single-crystal $SrTiO_3$, we demonstrate that the room-temperature incipient plastic deformation indicated by the indentation pop-in can be caused by purely dislocation-mediated plastic flow when the indenter tip radius is smaller than a critical value R_c. When R_c is exceeded, concurrent dislocation plasticity and crack formation will occur at such pop-in events. The theoretical justification and experimental validation suggest a new indentation size effect related to the size-dependent competition of dislocation/crack activities during pop-in events for brittle ceramic materials:

1. When the tip radius is sufficiently small ($R < R_c$), the maximum shear stress reaches the shear strength prior

to the maximum tensile stress or mode I fracture, so that the dislocation activation (nucleation, multiplication, and motion) is favored. Therefore, purely dislocation-mediated plasticity dominates during the indentation pop-in event, while crack formation is suppressed. By further increasing the load, cracks can be initiated by dislocation pileup beneath the indenter.

2. When the tip radius is sufficiently large ($R > R_c$), concurrent dislocation activity and crack formation would occur during the pop-in events due to the dynamic deformation process as well as increased probability of probing pre-existing flaws in the near surface, which may result in a more favorable situation for crack formation.

With further preliminary validation on three other advanced ceramic oxides (α-Al_2O_3, $BaTiO_3$, and TiO_2), the current study aims to serve as a guide for using nanoindentation as a feasible technique to study the dislocation-mediated incipient plasticity for brittle ceramic materials (beyond oxides) at micro-/nanoscale, including but not limited to quantification of pop-in statistics in ceramics[12,34] related to dislocation activation energy and activation volume,[103-105] and nanoindentation creep tests.[34] Such studies have not been comprehensively evaluated at room temperature or elevated temperatures due to the conventional belief that ceramics are brittle and susceptible to crack formation. Furthermore, our study also paves a path to introduce dislocations without forming cracks into oxides to facilitate the studies of dislocation-based functionalities.

ACKNOWLEDGMENTS

We thank S. Janocha and S. Bauer for the sample preparation, and Prof. A. Nakamura for providing the single-crystal $SrTiO_3$. X. F. thanks the financial support of Athene Young Investigator Programme (TU Darmstadt) and the Deutsche Forschungsgemeinschaft (DFG, No. 414179371). K. Ding thanks the DFG for financial support (FA 1662/1-1). G.D. and H.B. gratefully acknowledge funding by the ERC Advanced Grant GB-Correlate (Grant Agreement 787446). H.T. acknowledges her Ph.D. fellowship from the International Max Planck Research School for Interface Controlled Materials for Energy Conversion (IMPRS SurMat). K. Durst acknowledges the funding by DFG (DU 424/11-1). We gratefully acknowledge Prof. Jürgen Rödel (TU Darmstadt) and Prof. Brian Lawn for kindly reading through the manuscript and providing helpful comments. The helpful suggestions of the anonymous reviewers are also gratefully acknowledged. This paper is made Open Access under the German DEAL Agreement with support of Technical University of Darmstadt.

CONFLICT OF INTEREST

The authors declare no conflict of interest.

AUTHORS' CONTRIBUTIONS

X.F. designed the project and drafted the first manuscript. X.F., H.B., K. Ding, and H.T. performed the experiments and analyzed the data. E.B. performed the ECCI measurement on $BaTiO_3$ and interpreted the result. L.P., M.H., Y.L., G.D., and K. Durst discussed the results. All authors are involved in reading and revising the manuscript.

ORCID

Xufei Fang https://orcid.org/0000-0002-3887-0111
Hanna Bishara https://orcid.org/0000-0002-1353-7742
Lukas Porz https://orcid.org/0000-0003-3163-085X
Marion Höfling https://orcid.org/0000-0002-9387-9610
Yingwei Li https://orcid.org/0000-0002-8217-5511

REFERENCES

1. Lawn BR, Jensen T, Arora A. Brittleness as an indentation size effect. J Mater Sci. 1976;11:573–5.
2. Lawn BR, Marschall DB. Hardness, Toughness, and Brittleness: An Indentation Analysis. J Am Ceram Soc. 1979;62(7–8):340–7.
3. Lawn BR. Fracture and deformation in brittle solids: A perspective on the issue of scale. J Mater Res. 2004;19(1):22–9.
4. Lawn BR, Cook RF. Probing material properties with sharp indenters: a retrospective. J Mater Sci. 2012;47(1):1–22.
5. Gerberich WW, Stauffer DD, Beaber AR, Tymiak NI. A brittleness transition in silicon due to scale. J Mater Res. 2011;27(3):552–61.
6. Gerberich WW, Michler J, Mook WM, Ghisleni R, Östlund F, Stauffer DD, et al. Scale effects for strength, ductility, and toughness in "brittle" materials. J Mater Res. 2011;24(3):898–906.
7. Carter CB, Norton MG. Ceramic materials, 2nd edn. New York, NY: Springer; 2013.
8. Brunner D, Taeri-Baghbadrani S, Sigle W, Rühle M. Surprising results of a study on the plasticity in strontium titanate. J Am Ceram Soc. 2001;84(5):1161–3.
9. Argon AS, Orowan E. Plastic deformation in MgO single crystals. Phil Mag. 1964;9(102):1003–21.
10. Johnston WG, Gilman JJ. Dislocation velocities, dislocation densities, and plastic flow in lithium fluoride crystals. J Appl Phys. 1959;30(2):129–44.
11. Mark AF, Castillo-Rodríguez M, Sigle W. Unexpected plasticity of potassium niobate during compression between room temperature and 900°C. J Eur Ceram Soc. 2016;36(11):2781–93.
12. Nakamura A, Fang X, Matsubara A, Tochigi E, Oshima Y, Saito T, et al. Photoindentation: a new route to understanding dislocation behavior in light. Nano Lett. 2021;21:1962–7.
13. Nakamura A, Matsunaga K, Tohma J, Yamamoto T, Ikuhara Y. Conducting nanowires in insulating ceramics. Nat Mater. 2003;2(7):453–6.
14. Feng B, Ishikawa R, Kumamoto A, Shibata N, Ikuhara Y. Atomic scale origin of enhanced ionic conductivity at crystal defects. Nano Lett. 2019;19(3):2162–8.
15. Ikuhara Y. Nanowire design by dislocation technology. Prog Mater Sci. 2009;54(6):770–91.
16. Adepalli KK, Kelsch M, Merkle R, Maier J. Influence of line defects on the electrical properties of single crystal TiO_2. Adv Func Mater. 2013;23(14):1798–806.

17. Ren P, Höfling M, Koruza J, Lauterbach S, Jiang X, Frömling T, et al. High temperature creep-mediated functionality in polycrystalline barium titanate. J Am Ceram Soc. 2019;103(3):1891–902.
18. Kim SI, Lee KH, Mun HA, Kim HS, Hwang SW, Roh JW, et al. Dense dislocation arrays embedded in grain boundaries for high-performance bulk thermoelectrics. Science. 2015;348(6230):109–14.
19. Pan Y, Aydemir U, Grovogui JA, Witting IT, Hanus R, Xu Y, et al. Melt-centrifuged $(Bi, Sb)_2Te_3$: engineering microstructure toward high thermoelectric efficiency. Adv Mater. 2018;30:e1802016.
20. Khafizov M, Pakarinen J, He L, Hurley DH. Impact of irradiation induced dislocation loops on thermal conductivity in ceramics. J Am Ceram Soc. 2019;102(12):7533–42.
21. Li J, Wang H, Zhang X. Nanoscale stacking fault–assisted room temperature plasticity in flash-sintered TiO_2. Sci Adv. 2019;eaaw5519.
22. Cho J, Li J, Wang H, Li Q, Fan Z, Mukherjee AK, et al. Study of deformation mechanisms in flash-sintered yttria-stabilized zirconia by in-situ micromechanical testing at elevated temperatures. Mater Research Lett. 2019;7(5):194–202.
23. Adepalli KK, Yang J, Maier J, Tuller HL, Yildiz B. Tunable oxygen diffusion and electronic conduction in $SrTiO_3$ by dislocation-induced space charge fields. Adv Func Mater. 2017;27(22):1700243.
24. Ikuhara Y, Nishimura H, Nakamura A, Matsunaga K, Yamamoto T, Lagerloef KPD. Dislocation structures of low-angle and near-sigma 3 grain boundaries in alumina bicrystals. J Am Ceram Soc. 2003;86(4):595–602.
25. Takehara K, Sato Y, Tohei T, Shibata N, Ikuhara Y. Titanium enrichment and strontium depletion near edge dislocation in strontium titanate [001]/(110) low-angle tilt grain boundary. J Mater Sci. 2014;49(11):3962–9.
26. Choi SY, Kim SD, Choi M, Lee HS, Ryu J, Shibata N, et al. Assessment of strain-generated oxygen vacancies using $SrTiO_3$ bicrystals. Nano Lett. 2015;15(6):4129–34.
27. Kondo S, Mitsuma T, Shibata N, Ikuhara Y. Direct observation of individual dislocation interaction processes with grain boundary. Science Advances. 2016;2:e1501926.
28. Patterson EA, Major M, Donner W, Durst K, Webber KG, Rödel J. Temperature-dependent deformation and dislocation density in $SrTiO_3$ (001) single crystals. J Am Ceram Soc. 2016;99(10):3411–20.
29. Gumbsch P, Taeri-Baghbadrani S, Brunner D, Sigle W, Ruhle M. Plasticity and an inverse brittle-to-ductile transition in strontium titanate. Phys Rev Lett. 2001;87(8):085505.
30. Nakamura A, Yasufuku K, Furushima Y, Toyoura K, Lagerlöf K, Matsunaga K. Room-temperature plastic deformation of strontium titanate crystals grown from different chemical compositions. Crystals. 2017;7(11):351.
31. Oshima Y, Nakamura A, Matsunaga K. Extraordinary plasticity of an inorganic semiconductor in darkness. Science. 2018;360:772–4.
32. Fang X, Porz L, Ding K, Nakamura A. Bridging the gap between bulk compression and indentation test on room-temperature plasticity in oxides: case study on $SrTiO_3$. Crystals. 2020;10(10):933–47.
33. Johanning M, Porz L, Dong J, Nakamura A, Li J-F, Rödel J. Influence of dislocations on thermal conductivity of strontium titanate. Appl Phys Lett. 2020;117(2):021902.
34. Fang X, Ding K, Janocha S, Minnert C, Rheinheimer W, Frömling T, et al. Nanoscale to microscale reversal in room-temperature plasticity in $SrTiO_3$ by tuning defect concentration. Scripta Mater. 2020;188:228–32.
35. Javaid F, Bruder E, Durst K. Indentation size effect and dislocation structure evolution in (001) oriented $SrTiO_3$ Berkovich indentations: HR-EBSD and etch-pit analysis. Acta Mater. 2017;139:1–10.
36. Javaid F, Johanns KE, Patterson EA, Durst K. Temperature dependence of indentation size effect, dislocation pile-ups, and lattice friction in (001) strontium titanate. J Am Ceram Soc. 2018;101(1):356–64.
37. Gaillard Y, Tromas C, Woirgard J. Quantitative analysis of dislocation pile-ups nucleated during nanoindentation in MgO. Acta Mater. 2006;54(5):1409–17.
38. Montagne A, Tromas C, Audurier V, Woirgard J. A new insight on reversible deformation and incipient plasticity during nanoindentation test in MgO. J Mater Res. 2011;24(3):883–9.
39. Gaillard Y, Anglada M, Jiménez-Piqué E. Nanoindentation of yttria-doped zirconia: effect of crystallographic structure on deformation mechanisms. J Mater Res. 2011;24(3):719–27.
40. Lodes MA, Hartmaier A, Göken M, Durst K. Influence of dislocation density on the pop-in behavior and indentation size effect in CaF_2 single crystals: Experiments and molecular dynamics simulations. Acta Mater. 2011;59(11):4264–73.
41. Lawn BR, Borrero-Lopez O, Huang H, Zhang Y. Micromechanics of machining and wear in hard and brittle materials. J Am Ceram Soc. 2021;104:5–22.
42. Page TF, Oliver WC, McHargue CJ. The deformation behavior of ceramic crystals subjected to very low load (nano)indentations. J Mater Res. 2011;7(2):450–73.
43. Gaillard Y, Tromas C, Woirgard J. Study of the dislocation structure involved in a nanoindentation test by atomic force microscopy and controlled chemical etching. Acta Mater. 2003;51(4):1059–65.
44. Tromas C, Gaillard Y, Woirgard J. Nucleation of dislocations during nanoindentation in MgO. Phil Mag. 2006;86(33–35):5595–606.
45. Kucheyev SO, Bradby JE, Williams JS, Jagadish C, Swain MV. Mechanical deformation of single-crystal ZnO. Appl Phys Lett. 2002;80(6):956–8.
46. Javaid F, Stukowski A, Durst K. 3D Dislocation structure evolution in strontium titanate: Spherical indentation experiments and MD simulations. J Am Ceram Soc. 2017;100(3):1134–45.
47. Kondo S, Shibata N, Mitsuma T, Tochigi E, Ikuhara Y. Dynamic observations of dislocation behavior in $SrTiO_3$ by in situ nanoindentation in a transmission electron microscope. Appl Phys Lett. 2012;100:181906.
48. Hockey BJ, Lawn BR. Electron microscopy of microcracking about indentations in aluminium oxide and silicon carbide. J Mater Sci. 1975;10:1275–84.
49. Lawn BR, Hockey BJ, Richter H. Indentation analysis: application in the strength and wear of brittle materials. J Microsc. 1983;130:295–308.
50. Hockey BJ. Plastic deformation of aluminum oxide by indentation and abrasion. J Am Ceram Soc. 1971;54(5):223–31.
51. Li J, Dehm G, Kirchlechner C. How close can indents be placed without risking an erroneous pop-in statistics? Materialia. 2019;7:100378.
52. Zhang W, Gao Y, Xia Y, Bei H. Indentation Schmid factor and incipient plasticity by nanoindentation pop-in tests in hexagonal close-packed single crystals. Acta Mater. 2017;134:53–65.
53. Bei H, Gao YF, Shim S, George EP, Pharr GM. Strength differences arising from homogeneous versus heterogeneous dislocation nucleation. Phys Rev B. 2008;77(6):060103.
54. Morris JR, Bei H, Pharr GM, George EP. Size effects and stochastic behavior of nanoindentation pop in. Phys Rev Lett. 2011;106(16):165502.

55. Bei H, Xia YZ, Barabash RI, Gao YF. A tale of two mechanisms: strain-softening versus strain-hardening in single crystals under small stressed volumes. Scripta Mater. 2016;110:48–52.
56. Shim S, Bei H, George EP, Pharr GM. A different type of indentation size effect. Scripta Mater. 2008;59(10):1095–8.
57. Fang X, Kreter A, Rasinski M, Kirchlechner C, Brinckmann S, Linsmeier C, et al. Hydrogen embrittlement of tungsten induced by deuterium plasma: Insights from nanoindentation tests. J Mater Res. 2018;33(20):3530–6.
58. Gao Y, Bei H. Strength statistics of single crystals and metallic glasses under small stressed volumes. Prog Mater Sci. 2016;82:118–50.
59. Reddy KM, Guo D, Song S, Cheng C, Han J, Wang X, et al. Dislocation-mediated shear amorphization in boron carbide. Sci Adv. 2021;7(8):eabc6714.
60. Ma Y, Cao L, Hang W, Zhang T, Yuan J. Crystallographic orientation effect on the incipient plasticity and its stochastic behavior of a sapphire single crystal by spherical nanoindentation. Ceram Int. 2020;46(10):15554–64.
61. Gerberich WW, Nelson JC, Lilleodden ET, Anderson P, Wyrobek JT. Indentation induced dislocation nucleation: the initial yield point. Acta Mater. 1996;44(9):3585–98.
62. Lorenz D, Zeckzer A, Hilpert U, Grau P, Johansen H, Leipner HS. Pop-in effect as homogeneous nucleation of dislocations during nanoindentation. Phys Rev B. 2003;67(17):172101.
63. Fang X, Ding K, Minnert C, Nakamura A, Durst K. Dislocation-based crack initiation and propagation in single-crystal $SrTiO_3$. J Mater Sci. 2021;56:5479–92.
64. Yang K-H, Ho N-J, Lu H-Y. Plastic deformation of <001> single-crystal $SrTiO_3$ by compression at room temperature. J Am Ceram Soc. 2011;94(9):3104–11.
65. Wei J, Ogawa T, Feng B, Yokoi T, Ishikawa R, Kuwabara A, et al. Direct measurement of electronic band structures at oxide grain boundaries. Nano Lett. 2020;20(4):2530–6.
66. Adepalli KK, Kelsch M, Merkle R, Maier J. Enhanced ionic conductivity in polycrystalline TiO_2 by "one-dimensional doping". Phys Chem Chem Phys. 2014;16(10):4942–51.
67. Johnson KL. Contact mechanics. Cambridge, London: Cambridge University Press; 1985.
68. Frank FC, Lawn BR. On the theory of Hertzian fracture. Proc R Soc A: Mathematical, Phys Eng Sci. 1967;299(1458):291–307.
69. Hertzberg RW, Vinci RP, Hertzberg JL. Deformation and fracture mechanics of engineering materials, 5th edn. Westford, MA: Courier Westford; 2013.
70. Carpinteri A, Cornetti P, Pugno N, Sapora A, Taylor D. A finite fracture mechanics approach to structures with sharp V-notches. Eng Fract Mech. 2008;75(7):1736–52.
71. Cornetti P, Pugno N, Carpinteri A, Taylor D. Finite fracture mechanics: a coupled stress and energy failure criterion. Eng Fract Mech. 2006;73(14):2021–33.
72. Anderson TL. Fracture mechanics_fundamentals and applications. Boca Raton, FL: CRC Press; 2005.
73. Lawn B. Fracture of brittle solids, 2nd edn. Cambridge: Cambridge University Press; 1993.
74. Oliver WC, Pharr GM. An improved technique for determining hardness and elastic modulus using load and displacement sensing indentation experiments. J Mater Res. 1992;7(6):1564–83.
75. Gao H, Nix WD. Indentation size effects in crystalline materials: a law for strain gradient plasticity. J Mech Phys Solids. 1998;46(3):411–25.
76. Cook RF. Fracture sequences during elastic–plastic indentation of brittle materials. J Mater Res. 2019;34(10):1633–44.
77. Lawn BR, Padture NP, Cai H, Guiberteau F. Making ceramics "Ductile". Science. 1994;263:1114.
78. Hagan JT, Swain MV. The origin of median and lateral cracks around plastic indents in brittle materials. J Phys D Appl Phys. 1978;11:2091.
79. Hagan JT. Micromechanics of crack nucleation during indentations. J Mater Sci. 1979;14:1975–2980.
80. Lathabai S, Rödel J, Dabbs T, Lawn BR. Fracture mechanics model for subthreshold indentation flaws: part I equilibrium fracture. J Mater Sci. 1991;26:2157–68.
81. Lawn B, Dabbs TP, Fairbanks CJ. Kinetics of shear-activated indentation crack initiation in soda-lime glass. J Mater Sci. 1983;18:2785–97.
82. Bradby JE, Williams JS, Wong-Leung J, Swain MV, Munroe P. Mechanical deformation in silicon by micro-indentation. J Mater Res. 2001;16(5):1500–7.
83. Bradby JE, Williams JS, Swain MV. Pop-in events induced by spherical indentation in compound semiconductors. J Mater Res. 2004;19(1):380–6.
84. Hirth JP, Lothe J. Theory of dislocations, 2nd edn. Malabar, FL: John Wiley & Sons Inc.; 1982.
85. Groves GW, Kelly A. Independent slip systems in crystals. Phil Mag. 1963;8(89):877–87.
86. Farber BY, Chiarelli AS, Heuer AH. A dislocation mechanism of crack nucleation in cubic zirconia single crystals. Philos Mag A. 1994;70(1):201–17.
87. Stokes RJ, Johnston TL, Li CH. Crack formation in magnesium oxide single crystals. Phil Mag. 1958;3(31):718–25.
88. Argon AS, Orowan E. Crack nucleation in MgO single crystals. Phil Mag. 1964;9(102):1023–39.
89. Stroh AN. A theory of the fracture of metals. Adv Phys. 1957;6(24):418–65.
90. Suratwala T. Materials science and technology of optical fabrication, 1st edn. Hoboken, NJ: John Wiley & Sons; 2018.
91. Sudharshan Phani P, Oliver WC. Critical examination of experimental data on strain bursts (pop-in) during spherical indentation. J Mater Res. 2020;35(8):1028–36.
92. Gaillard Y, Tromas C, Woirgard J. Pop-in phenomenon in MgO and LiF: observation of dislocation structures. Philos Mag Lett. 2010;83(9):553–61.
93. Page TF, Riester L, Hainsworth SV. The plasticity response of 6H-SiC and related isostructural materials to nanoindentation: slip vs densification. Mat Res Soc Symp Proc. 1998;522:113–8.
94. Guicciardi S, Melandri C, Monteverde FT. Characterization of pop-in phenomena and indentation modulus in a polycrystalline ZrB_2 ceramic. J Eur Ceram Soc. 2010;30(4):1027–34.
95. Gruber M, Leitner A, Kiener D, Supancic P, Bermejo R. Incipient plasticity and surface damage in $LiTaO_3$ and $LiNbO_3$ single crystals. Mater Des. 2018;153:221–31.
96. Östlund F, Rzepiejewska-Malyska K, Leifer K, Hale LM, Tang Y, Ballarini R, et al. Brittle-to-ductile transition in uniaxial compression of silicon pillars at room temperature. Adv Func Mater. 2009;19(15):2439–44.
97. Nowak R, Chrobak D, Nagao S, Vodnick D, Berg M, Tukiainen A, et al. An electric current spike linked to nanoscale plasticity. Nat Nanotechnol. 2009;4(5):287–91.
98. Chrobak D, Nordlund K, Nowak R. Nondislocation origin of GaAs nanoindentation pop-in event. Phys Rev Lett. 2007;98(4):045502.

99. Mann AB, van Heerden D, Pethica JB, Weihs TP. Size-dependent phase transformations during point loading of silicon. J Mater Res. 2000;15(8):1754–8.
100. Pharr GM, Oliver WC, Harding DS. New evidence for a pressure-induced phase transformation during the indentation of silicon. J Mater Res. 1991;6(6):1129–30.
101. Gouldstone A, Chollacoop N, Dao M, Li J, Minor A, Shen Y. Indentation across size scales and disciplines: Recent developments in experimentation and modeling. Acta Mater. 2007;55(12):4015–39.
102. Minor AM, Lilleodden ET, Jin M, Stach EA, Chrzan DC, Morris JJW. Room temperature dislocation plasticity in silicon. Phil Mag. 2005;85(2–3):323–30.
103. Schuh CA, Mason JK, Lund AC. Quantitative insight into dislocation nucleation from high-temperature nanoindentation experiments. Nat Mater. 2005;4(8):617–21.
104. Mason JK, Lund AC, Schuh CA. Determining the activation energy and volume for the onset of plasticity during nanoindentation. Phys Rev B. 2006;73(5):054102.
105. Ma Y, Huang X, Hang W, Liu M, Song Y, Yuan J, et al. Nanoindentation size effect on stochastic behavior of incipient plasticity in a $LiTaO_3$ single crystal. Eng Fract Mech. 2020;226.

SUPPORTING INFORMATION

Additional supporting information may be found online in the Supporting Information section.

How to cite this article: Fang X, Bishara H, Ding K, et al. Nanoindentation pop-in in oxides at room temperature: Dislocation activation or crack formation?. *J Am Ceram Soc*. 2021;104:4728–4741. https://doi.org/10.1111/jace.17806